Rapid Communications

Tuning a regular cavity to wave chaos with metasurface-reconfigurable walls

Jean-Baptiste Gros [*] and Philipp del Hougne [†]
Institut Langevin, CNRS UMR 7587, ESPCI Paris, PSL Research University, 75005 Paris, France

Geoffroy Lerosey
Greenerwave, ESPCI Paris Incubator PC'up, 75005 Paris, France

(Received 6 March 2020; accepted 22 April 2020; published 1 June 2020)

Wave-chaotic systems underpin a wide range of research activities from fundamental studies of quantum chaos via electromagnetic compatibility up to more recently emerging applications, such as microwave imaging for security screening, antenna characterization, or wave-based analog computation. To implement a wave-chaotic system experimentally, traditionally cavities of elaborate geometries (bow tie shapes, truncated circles, or parallelepipeds with hemispheres) are employed because the geometry dictates the wave field's characteristics. Here, we propose and experimentally verify a conceptually different approach: a cavity of regular geometry but with tunable boundary conditions, experimentally implemented by leveraging a reconfigurable metasurface reflect array. This approach offers an alternative stirring mechanism and enables a fuller study of random matrix theory in connection with wave chaos.

DOI: 10.1103/PhysRevA.101.061801

For decades, wave chaos has been an attractive field of fundamental research concerning a wide variety of physical systems, such as quantum physics [1–4], room or ocean acoustics [5–7], elastodynamics [8], guided-wave optics [9], or microwave cavities [10–14]. The success of wave chaos is mainly due to its ability to describe such a variety of complex systems through a unique formalism yielding a universal statistical behavior. Indeed, since the Bohigas-Giannoni-Schmit conjecture [15] concerning the universality of level fluctuations in chaotic quantum spectra, it has become customary to analyze spectral and spatial statistics of wave systems whose ray counterpart is chaotic with the help of statistical tools introduced by random matrix theory (RMT) [12,16–20]. In recent years, electromagnetic (EM) chaotic cavities have been involved in a variety of applications ranging from reverberation chambers (RCs) for electromagnetic compatibility (EMC) tests [21–27] via wavefront shaping [28–30] and microwave imaging [31–35] to applications in telecommunication and energy harvesting [36,37], indoor sensing [38,39], antenna characterization [40], and wave-based analog computation [41]. All of these applications leverage the field ergodicity [42] of responses and eigenfields of chaotic cavities [20,22]. Traditionally, whether they are used to study fundamental physics or for applications, these cavities are associated with irregular geometries. They are often built from a parallelepipedic cavity by modifying its geometry (for instance, by adding spherical caps or hemispheres [11,21,22,24,43]) so that its spatial and/or spectral statistics follow the universal RMT predictions [22]. Furthermore, most of these cavities include mechanically movable elements, so-called stirrers, adding to the chaoticity, and allowing one to perform ensemble averaging (mode stirring) [44,45].

Here, we investigate a completely different approach to build a chaotic cavity by *only* modulating locally the boundary conditions of a cavity of regular geometry. Experimentally, the tuning of the boundary conditions is achieved with a reconfigurable metasurface reflect array that covers parts of the cavity walls. First, we study the amount of metasurface elements required to tune a regular cavity to wave chaos. Since the metasurface is built upon resonant elements, we consider frequencies matching their operation band. The chaoticity of the cavity is evaluated by comparing the *experimentally* observed wave field distribution with RMT predictions for wave-chaotic systems. The latter depend on a single experimentally evaluable parameter: the mean modal overlap d [20,46]. This overlap is defined at the operating frequency f as the product of the average modal bandwidth Γ_f and the mean density of states n_f. Second, by using an unexpected efficiency of the metasurfaces outside their operation band, we implement our approach in different regimes of modal overlap, the latter being a key parameter of all wave systems [20,29,47,48].

Experimental setup. For our experiments, we cover three contiguous and nonparallel walls of a metallic parallelepipedic cavity ($42 \times 38.5 \times 35$ cm^3) with electronically reconfigurable metasurfaces (ERMs) [49] without significantly altering the cavity geometry (see Fig. 1). Each of the three metasurfaces consists of 76 phase-binary pixels. The underlying working principle of hybridizing two resonances is outlined in Ref. [50]. By controlling the bias voltage of a *p-i-n* diode, each pixel can individually be configured to emulate the behavior of a quasiperfect electric or quasiperfect magnetic conductor. Stated differently, the phase of the tangential

[*] jean-baptiste.gros@espci.fr
[†] Present address: Institut de Physique de Nice, CNRS UMR 7010, Université Côte d'Azur, 06100 Nice, France.

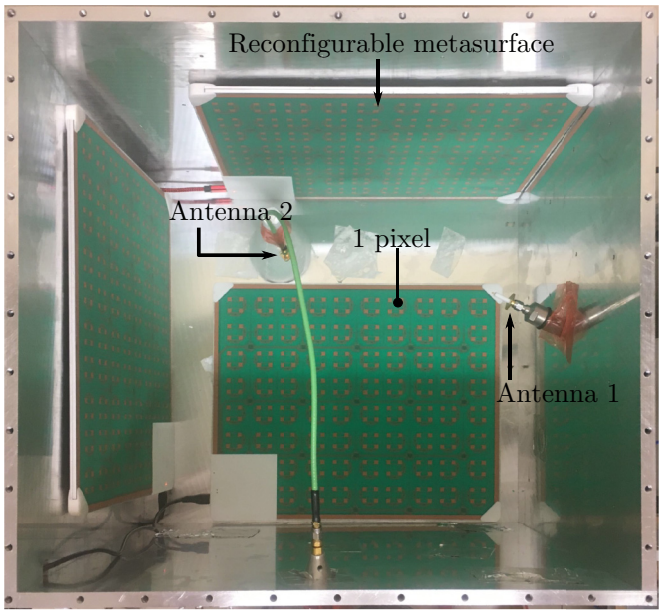

FIG. 1. Top view of the metallic parallelepipedic cavity ($42 \times 38.5 \times 35$ cm^3). Three walls are covered by reconfigurable metasurfaces (76 pixels per metasurface). Each metasurface pixel can be configured electronically to emulate a perfect electric or magnetic conductor. The wave field is probed by measuring the transmission between two antennas with a vector network analyzer (VNA). The VNA and the cavity's top plate are not shown in this figure.

component of the field reflected by the pixel can be shifted by π. Note that our proposal to locally modulate the cavity's boundary conditions could also be implemented with other designs of tunable impedance surfaces, such as mushroom structures [31,51–53]. Since the design of our metasurface leverages resonant effects, the band of frequencies over which it displays the desired effect is *a priori* inherently limited. The ERM prototype we use for our experiments has been designed to work efficiently within a 1-GHz bandwidth around 5.2 GHz.

Random matrix theory benchmark. To evaluate whether boundary condition modulations induced by ERMs can tune a regular cavity to wave chaos, we compare the statistical distribution of the normalized intensity I of Cartesian field components measured for a given ensemble of ERM configurations with the theoretical RMT distribution. In this section, we recall the main steps leading to the RMT prediction [20,46,54].

In the presence of losses, for a given configuration of an ideal chaotic cavity (or a given frequency, relying on ergodicity), the real and imaginary parts of each Cartesian component of the field are independently Gaussian distributed but with different variances [20,22]. The ensuing distribution of the modulus square of each component $|E_a|^2$ depends on a single parameter ρ, called the *phase rigidity*, defined by [20]

$$\rho = \frac{\int_V \vec{E}\cdot\vec{E}\,d\vec{r}}{\int_V ||\vec{E}||^2 d\vec{r}}. \tag{1}$$

More precisely, in a chaotic RC, due to the ergodicity of the modes contributing to the response, for a given excitation frequency and a given configuration (here, ERMs configurations, polarizations, and positions of the antennas), the probability distribution of the normalized intensity of the Cartesian component $I = |E_a|^2/\langle|E_a|^2\rangle_{\vec{r}}$ depends solely on the modulus of ρ and is given by [20,55]

$$P(I;\rho) = \frac{1}{\sqrt{1-|\rho|^2}} \exp\left[-\frac{I}{1-|\rho|^2}\right] \mathcal{I}_0\left[\frac{|\rho| I}{1-|\rho|^2}\right], \tag{2}$$

with $\mathcal{I}_0$ being the modified Bessel function of the first kind. This result was originally proposed by Pnini and Shapiro [56] to model the statistics of scalar fields in partially open chaotic systems.

The above distribution continuously interpolates between the two extreme distributions, namely, Porter-Thomas for lossless closed systems ($|\rho| \to 1$) and exponential for completely open systems ($|\rho| = 0$). The latter case corresponds to the limit where the field is statistically equivalent to a random superposition of traveling plane waves [20,56] meaning that real and imaginary parts of each Cartesian component of the field are statistically independent and identically distributed following a normal distribution. This regime is known as Hill's regime in the EMC community [45,57], Ericson's regime in nuclear physics [58], or Schroeder's regime in room acoustics [5] and corresponds to a very high modal overlap regime.

Since the phase rigidity is itself a distributed quantity, the distribution of the normalized field intensity in a chaotic RC for an ensemble of responses resulting from stirring reads

$$P_I(I) = \int_0^1 P_\rho(\rho) P(I;\rho) d\rho, \tag{3}$$

where $P_\rho(\rho)$ is the distribution of the phase rigidity of the responses. Preliminary investigations, based on numerical simulations of the random matrix model described in Ref. [20], show that $P_\rho(\rho)$ depends only on the mean modal overlap d. An ansatz was proposed in Ref. [46] to determine $P_\rho(\rho)$ solely based on the knowledge of d. This ansatz reads

$$P_\rho^W(\rho) = \frac{2B\,\exp[-2B\rho/(1-\rho)]}{(1-\rho)^2}, \tag{4}$$

where the parameter B has a smooth d dependence [46] numerically deduced from the RMT model presented in Ref. [20]. Originally, in Ref. [46], the empirical estimation of $B(d)$ was limited to $d \leqslant 1$. Currently, $B(d)$ has been extended to larger values of d and is given by [54]

$$B(d) = \frac{ad^2}{1+bd+cd^2}, \tag{5}$$

with $a = 0.50 \pm 0.02$, $b = 1.35 \pm 0.03$, and $c = 0.30 \pm 0.02$ [54]. The mean modal overlap d is, therefore, the key parameter to predict the statistical distribution of the normalized intensity I of Cartesian field components,

$$P_{I;d}(I) = \int_0^1 P_\rho^W(\rho) P(I;\rho) d\rho. \tag{6}$$

For a three-dimensional (3D) EM cavity of volume V, the mean density of states can be estimated with Weyl's law,

which reads at leading order $n_f \simeq n_w(f) = 8\pi V c^{-3} f^2$ [59], where c is the speed of light and f is the mean of the considered frequency window. The mean modal overlap d is, thus, related to f, V, the modal width Γ_f, and the composite quality factor $Q = f/\Gamma_f$ through

$$d = n_f \Gamma_f \simeq \frac{8\pi V}{c^3 Q} f^3. \tag{7}$$

Minimum number of "activated" ERM pixels. First, we are interested in the minimum number of metasurface pixels that have to emulate a perfect magnetic conductor (PMC) to observe wave-chaotic behavior in a cavity with regular geometry. To that end, we choose 500 random configurations of the three ERMs for which the overall number of PMC-like (activated) pixels n_a is fixed and the $228 - n_a$ remaining pixels are left in their PEC-like state (not activated). For each configuration, we measure the S parameters between two monopole antennas for 1601 frequency points in a frequency window of 250 MHz around 5.2 GHz where the pixels are the most efficient. This experiment is repeated for different values of $n_a \in [2, 122]$. Then, for each set of experiments with fixed n_a, we extract for both antennas their frequency-dependent coupling constants $\kappa_i(f)$ which read [12,43,60,61]

$$\kappa_i = \frac{|1 - \langle S_{ii}\rangle|^2}{1 - |\langle S_{ii}\rangle|^2} \qquad (i = 1, 2), \tag{8}$$

where $S_{ii}(f)$ $(i = 1, 2)$ are the reflection parameters and $\langle\cdot\rangle$ denotes an ensemble average over random ERM configurations. Next, we deduce from the measurement of the transmission parameter $S_{12}(f)$ the normalized value of the amplitude of the Cartesian component of the electric field along the orientation of the monopole antenna 2 inside the cavity as [46]

$$E_a = \vec{E}(\vec{r}_2, f) \cdot \hat{n}_a = \frac{S_{12}(f)}{\kappa_1 \kappa_2}, \tag{9}$$

where $\vec{E}(\vec{r}_2, f)$ is the electric field at the position of antenna 2 and $\hat{n}_a$ is the unit vector along the polarization of antenna 2.

The RMT prediction in Eq. (6) assumes that $\langle E_a\rangle$ is vanishing. Physically, this means that static contributions, such as direct processes (short path) are negligible [58,62–65]. Reasons for the presence of static contributions include directivity and relative positions of the antennas as well as the ERMs' stirring efficiency. To extract the universal properties from our experiments that can be compared with RMT predictions, we numerically suppress the nonuniversal static contribution via the commonly used transformation $E_a \to E_a - \langle E_a\rangle$ [23,58]. In many practical applications involving reconfigurable wave chaos, such a differential approach to remove the static contribution is applied to efficiently use the available degrees of freedom [34,39,41,66]. The universal and nonuniversal contributions in our data are discussed and displayed in detail in the Supplemental Material [67].

For each set of experiments with fixed n_a, we compare the empirical cumulative distribution function (ECDF) of the normalized field intensity $I = |E_a|^2/\langle|E_a^2|\rangle$ of the ensemble of cavity configurations $F_{n_a}(I)$ with the theoretical cumulative distribution function,

$$F_{I;d}(I) = \int_0^I P_{I;d}(x)dx, \tag{10}$$

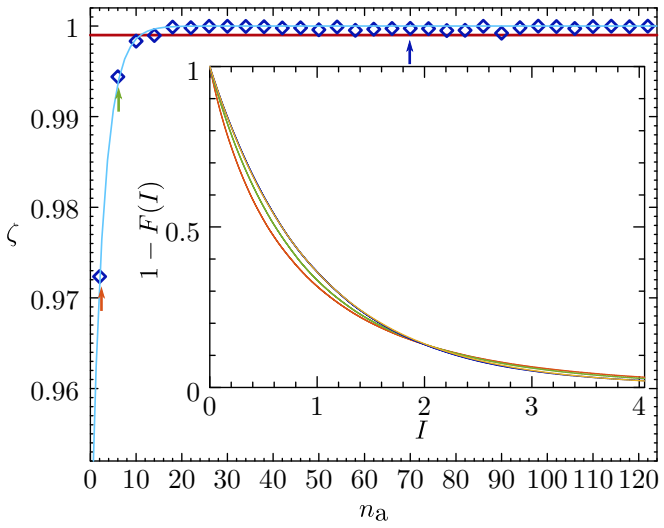

FIG. 2. Transition to chaotic behavior as the number of pixels emulating a perfect magnetic conductor n_a increases. Main plot: $\diamond$, blue continuous curve and red dotted line show, respectively, the experimental values of $\zeta(n_a)$ (see the text for details), the interpolation of $\zeta(n_a)$ by the heuristic function $f(x) = 1 - 0.06\exp(-0.373x)$ and the limit $\zeta = 0.999$ above which $F_{n_a}(I)$ is in good agreement with $F_{I;d}(I)$. The inset: red dashed-dotted line, green dotted line, blue continuous lines, and orange dashed line correspond, respectively, to $F_2(I)$, $F_6(I)$, $F_{70}(I)$, and $F_{I;d}(I)$. Arrows in the main plot locate the associated values of $\zeta(n_a)$.

where we use the experimentally obtained value of d. To estimate d with Eq. (7), we extract from our data the cavity's composite Q factor as $Q = f/\Gamma_f = 2\pi\tau f$, where $\tau = (2\pi\Gamma_f)^{-1}$ is the intensity decay time of the inverse Fourier-transformed transmission signal $|\mathrm{FT}(S_{21})|^2 \propto \exp(-t/\tau)$. Around 5.2 GHz, we thereby estimate $d = 19.81$. The deviation of the measured ECDF of field intensity $F_{n_a}(I)$ from the RMT prediction $F_{I;d}(I)$ with $d = 19.81$ is then estimated as

$$\zeta(n_a) = 1 - \left\langle \left(F_{n_a} - F_{I;d}\right)^2 \right\rangle_I / \left\langle \left(F_{n_a} - F_{n_a}\right)^2 \right\rangle_I. \tag{11}$$

In Fig. 2, the diamonds ($\diamond$) present the experimentally obtained values of $\zeta(n_a)$. Good agreement between the empirical $F_{n_a}(I)$ and the RMT prediction $F_{I;d}(I)$ is guaranteed as soon as $\zeta(n_a) \geqslant 0.999$. This is illustrated in the inset of Fig. 2 with the ECDFs $F_2(I)$, $F_6(I)$, and $F_{70}(I)$ corresponding, respectively, to cases of $\zeta < 0.99$, $0.99 \leqslant \zeta < 0.999$, and $\zeta \geqslant 0.999$. Among the three ECDFs shown, only $F_{70}(I)$ (which yields $\zeta \geqslant 0.999$) is in good agreement with the RMT prediction $F_{I;d}(I)$. To estimate the minimum number of activated pixels $n_{\min}$, required to obtain a chaotic cavity, we interpolate the experimental $\zeta(n_a)$ values by a heuristic function $f(x) = 1 - a\exp(-cx)$ and search the value $x_{\min}$ such that $f(x_{\min}) = 0.999$. The fit yields $a = 0.06 \pm 3.1\%$, $c = 0.373 \pm 3.4\%$, and $x_{\min} \simeq 10.98$. Therefore, for the specific cavity and metasurface design used in our experiment, $n_{\min} = 11$.

Extension to different modal overlap regimes. Having demonstrated that, in a regular cavity equipped with ERMs chaotic behavior can be observed within the ERMs' operation band, we now consider frequencies outside this band which allows us to explore different regimes of modal overlap. The

ERM pixels are individually less efficient far outside their designed operating band: The phase difference between the two states is well below π. Nonetheless, surprisingly, we observe that collectively they are still able to sufficiently alter the boundary conditions to observe wave-chaotic behavior. We now choose 9000 fully random configurations of the 228 pixels. For each ERM configuration, we measure the S parameters between the monopole antennas for 1601 frequency points in [1.8, 5.8 GHz]. At this point, we draw the reader's attention to the fact that most of RMT predictions assume that the mean density of states, the coupling strength of the antenna, the absorption and the ensuing mean modal overlap are constant [12,16–18,22,23,43,46,58,60,68–72]. Practically, this means that we assume that these quantities vary only slightly within the investigated frequency range. Obviously, in the present Rapid Communication, none of the above-mentioned parameters are slightly varying across the full frequency range from 1.8 to 5.8 GHz, especially the mean density of states. Therefore, we focus our study on a subset of five frequency windows of 150-MHz width, respectively, centered on 1.84, 3.1, 3.6, 4.5, and 5.2 GHz. The corresponding measured values of modal overlap are, respectively, $d = 0.4,\ 1.98,\ 3.47,\ 6.45$, and 19.81.

We can now study the field intensity distribution of the ensemble of random cavity configurations and thereby the chaoticity for different modal overlap regimes ranging from low modal overlap ($d < 1$) to very high modal overlap ($d \simeq 20 \gg 1$) [67]. For each frequency window, we compare as before the measured ECDF of the normalized field intensity with the theoretical cumulative distribution function $F_{I;d}$, given by Eq. (10) using the corresponding experimentally measured value of d. The results are shown in Fig. 3 where each continuous and dashed curve with the same color corresponds, respectively, to the complementary ECDF, $1 - F(I)$, of experimental data, and the RMT prediction $1 - F_{I;d}(I)$ [Eq. (10)] with d extracted from the experimental data. From the very low modal overlap regime with $d = 0.4$ (dark blue curves in Fig. 3) to the very high modal overlap regime with $d = 19.81$ (light blue curves in Fig. 3), we observe very good agreement over four decades between the ECDF of the normalized field intensity of the ensemble of cavity configurations and the RMT prediction for chaotic cavities. Hence, the cavity in Fig. 1 displays the universal statistical behavior expected in chaotic cavities when we randomly modulate its boundary conditions.

We note that, for higher values of d, the ECDFs of the experimental data are increasingly close to the cumulative distribution function for the Hill-Ericson-Schroeder regime (dotted purple curves in Fig. 3). The latter corresponds to the limit of very high modal overlap [5,45,57,58]. Nevertheless, because of the large size of the statistical uncorrelated sample ($\sim 5 \times 10^5$ transmission parameters per frequency window obtained by modulating the boundary condition of the cavity with ERMs), we can still discriminate between the RMT prediction and the Hill-Ericson-Schroeder regime—mainly on the tail of the distribution [73]. This is the case even for the largest modal overlap regime with $d \sim 20$ studied here. We note that having an equivalent size of an uncorrelated statistical sample with conventional mechanical stirring is much more difficult. Generally, the size of the statistical ensemble is between one and two orders of magnitude smaller [57,74].

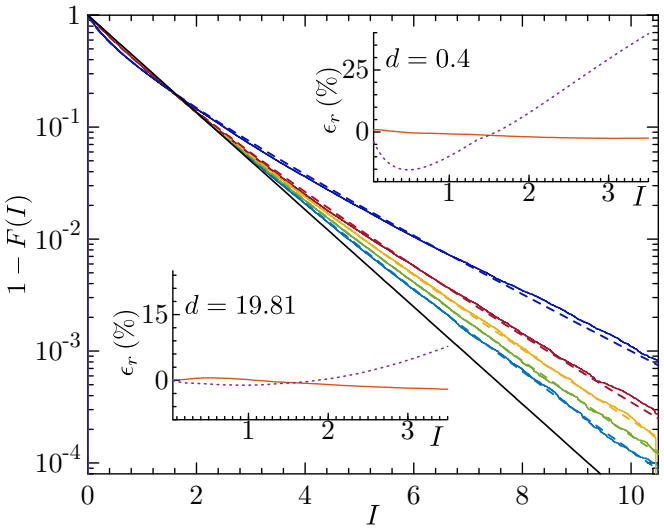

FIG. 3. For different regimes of modal overlap d, we compare the measured ECDF of normalized field intensity $F(I)$ (continuous curves) with the RMT prediction $F_{I;d}(I)$ given by Eq. (10) (dashed curve). The colors, in ascending order, correspond to $d =$ 19.81, 6.45, 3.47, 1.98, and 0.40. For reference, the cumulative distribution of the Hill-Ericson-Schroeder regime is also indicated (dotted purple). For the two extreme cases of $d = 0.4$ and $d = 19.81$, the two insets show the relative error ϵ_r between the ECDF and the RMT prediction (continuous red) as well as the Hill-Ericson-Schroeder regime (dotted purple).

Concluding remarks. Our Rapid Communication shows that a regular cavity equipped with reconfigurable metasurface reflect arrays can both (i) be tuned to wave chaos and (ii) stirred using an ensemble of random metasurface configurations. In the EMC community, a related proposal for an electronically reconfigurable RC has previously been proposed [44,75] and is experimentally demonstrated here. Reference [76] recently proposed to use a metasurface to improve the field uniformity in a reverberation chamber, an objective closely related to that of tuning a cavity to wave chaos [21,22,46]; however, the ability to simultaneously stir the field is lacking in Ref. [76] since the considered metasurface was not reconfigurable. At the same time, several papers in the area of sensing [31,34,35,38,39] used an ensemble of random configurations of an electronically reconfigurable chaotic cavity to stir the field but did not tune a regular cavity to wave chaos.

To summarize, we experimentally showed that random modulations of a regularly shaped cavity's boundary conditions with simple metasurfaces constitute an approach to construct a chaotic RC without mechanical modifications. Although mechanical modifications that do not sufficiently impact the overall geometry can lead to a nonfully chaotic cavity [21,22,24], our approach ensures that chaotic behavior can be observed provided that the amount of pixels in distinct states is sufficiently large. Furthermore, we have demonstrated that our approach enables the observation of chaotic behavior for a wide range of modal overlap regimes. Simultaneously,

we have thereby also presented an experimental verification of the validity of the RMT prediction of field intensity distribution [Eq. (6)] for modal overlaps much larger than unity. Originally, this prediction was proposed for weak-to-moderate modal overlap regime ($d \lesssim 1$) [20].

From a practical point of view, in a forthcoming paper [77], we will demonstrate how our approach offers access to a large number of uncorrelated cavity configurations which is an important feature for many applications leveraging chaotic reverberation chambers from computational imaging [31,32] or wave-based analog computation [41] via wireless environments [37,78–80] and antenna characterization [81–85] to EMC tests [86–89]. From a more fundamental point of view, thanks to our technique's ability to easily and rapidly access a very large amount of realizations, these reconfigurable chaotic cavities will enable a fuller study of RMT and could be used to verify recent predictions [68,90].

Acknowledgments. The authors thank O. Legrand, U. Kuhl, and F. Mortessagne from the Université Côte d'Azur for fruitful discussions and acknowledge funding from the French "Ministère des Armées, Direction Générale de l'Armement."

[1] *Les Houches 1989-Session LII: Chaos and Quantum Physics*, edited by M. J. Giannoni, A. Voros, and J. Zinn-Justin (North-Holland, Amsterdam, 1991).

[2] J. J. M. Verbaarschot, H. A. Weidenmüller, and M. R. Zirnbauer, Grassmann integration in stochastic quantum physics: The case of compound-nucleus scattering, Phys. Rep. **129**, 367 (1985).

[3] M. V. Berry, Regular and irregular semiclassical wavefunctions, J. Phys. A **10**, 2083 (1977).

[4] M. Lombardi and T. H. Seligman, Universal and nonuniversal statistical properties of levels and intensities for chaotic rydberg molecules, Phys. Rev. A **47**, 3571 (1993).

[5] F. Mortessagne, O. Legrand, and D. Sornette, Transient chaos in room acoustics, Chaos **3**, 529 (1993).

[6] Y. Aurégan and V. Pagneux, Acoustic scattering in duct with a chaotic cavity, Acta Acust. Acust. **102**, 869 (2016).

[7] S. Tomsovic and M. G. Brown, Ocean acoustics: A novel laboratory for wave chaos, in *New Directions in Linear Acoustics and Vibration; Quantum Chaos, Random Matrix Theory and Complexity*, edited by M. Wright and R. Weaver (Cambridge University Press, Cambridge, U.K., 2010), Chap. 11, pp. 169–183.

[8] O. I. Lobkis and R. L. Weaver, Complex modal statistics in a reverberant dissipative body, J. Acoust. Soc. Am. **108**, 1480 (2000).

[9] V. Doya, O. Legrand, F. Mortessagne, and C. Miniatura, Speckle statistics in a chaotic multimode fiber, Phys. Rev. E **65**, 056223 (2002).

[10] H.-J. Stöckmann and J. Stein, "Quantum" Chaos in Billiards Studied by Microwave Absorption, Phys. Rev. Lett. **64**, 2215 (1990).

[11] S. Deus, P. M. Koch, and L. Sirko, Statistical properties of the eigenfrequency distribution of three-dimensional microwave cavities, Phys. Rev. E **52**, 1146 (1995).

[12] U. Kuhl, O. Legrand, and F. Mortessagne, Microwave experiments using open chaotic cavities in the realm of the effective hamiltonian formalism, Fortschr. Phys. **61**, 404 (2013).

[13] B. Dietz and A. Richter, Quantum and wave dynamical chaos in superconducting microwave billiards, Chaos **25**, 097601 (2015).

[14] J. Barthélemy, O. Legrand, and F. Mortessagne, Complete *s* matrix in a microwave cavity at room temperature, Phys. Rev. E **71**, 016205 (2005).

[15] O. Bohigas, M. J. Giannoni, and C. Schmit, Characterization of Chaotic Quantum Spectra and Universality of Level Fluctuation Laws, Phys. Rev. Lett. **52**, 1 (1984).

[16] H.-J. Stöckmann, *Quantum Chaos: An Introduction* (Cambridge University Press, Cambridge, U.K., 1999).

[17] T. Guhr, A. Müller-Groeling, and H. A. Weidenmüller, Random-matrix theories in quantum physics: common concepts, Phys. Rep. **299**, 189 (1998).

[18] V. V. Sokolov and V. G. Zelevinsky, Dynamics and statistics of unstable quantum states, Nucl. Phys. A **504**, 562 (1989).

[19] I. Rotter, A non-Hermitian Hamilton operator and the physics of open quantum systems, J. Phys. A: Math. Theor. **42**, 153001 (2009).

[20] J.-B. Gros, U. Kuhl, O. Legrand, and F. Mortessagne, Lossy chaotic electromagnetic reverberation chambers: Universal statistical behavior of the vectorial field, Phys. Rev. E **93**, 032108 (2016).

[21] J.-B. Gros, U. Kuhl, O. Legrand, F. Mortessagne, O. Picon, and E. Richalot, Statistics of the electromagnetic response of a chaotic reverberation chamber, Adv. Electromagn. **4**, 38 (2015).

[22] J.-B. Gros, O. Legrand, F. Mortessagne, E. Richalot, and K. Selemani, Universal behavior of a wave chaos based electromagnetic reverberation chamber, Wave Motion **51**, 664 (2014).

[23] G. Gradoni, J.-H. Yeh, B. Xiao, T. M. Antonsen, S. M. Anlage, and E. Ott, Predicting the statistics of wave transport through chaotic cavities by the random coupling model: A review and recent progress, Wave Motion **51**, 606 (2014).

[24] L. Bastianelli, G. Gradoni, F. Moglie, and V. M. Primiani, Full wave analysis of chaotic reverberation chambers, in *2017 XXXIInd General Assembly and Scientific Symposium of the International Union of Radio Science (URSI GASS), Montreal, 2017* (IEEE, Piscataway, NJ. 2017), pp. 1–4.

[25] L. R. Arnaut, Operation of electromagnetic reverberation chambers with wave diffractors at relatively low frequencies, IEEE Trans. Electromagn. Compat. **43**, 637 (2001).

[26] F. Sarrazin and E. Richalot, Cavity modes inside a mode-stirred reverberation chamber extracted using the matrix pencil method, in *2017 11th European Conference on Antennas and Propagation (EUCAP), Paris, 2017* (IEEE, Piscataway, NJ, 2017), pp. 620–6221–4.

[27] G. Orjubin, E. Richalot, O. Picon, and O. Legrand, Wave chaos techniques to analyze a modeled reverberation chamber, C. R. Phys. **10**, 42 (2009).

[28] N. Kaina, M. Dupré, G. Lerosey, and M. Fink, Shaping complex microwave fields in reverberating media with binary tunable metasurfaces, Sci. Rep. **4**, 6693 (2015).

[29] M. Dupré, P. del Hougne, M. Fink, F. Lemoult, and G. Lerosey, Wave-Field Shaping in Cavities: Waves Trapped in a Box with Controllable Boundaries, Phys. Rev. Lett. **115**, 017701 (2015).

[30] P. del Hougne, F. Lemoult, M. Fink, and G. Lerosey, Spatiotemporal Wave Front Shaping in a Microwave Cavity, Phys. Rev. Lett. **117**, 134302 (2016).

[31] T. Sleasman, M. F. Imani, J. N. Gollub, and D. R. Smith, Microwave Imaging Using a Disordered Cavity with a Dynamically Tunable Impedance Surface, Phys. Rev. Appl. **6**, 054019 (2016).

[32] A. C. Tondo Yoya, B. Fuchs, and M. Davy, Computational passive imaging of thermal sources with a leaky chaotic cavity, Appl. Phys. Lett. **111**, 193501 (2017).

[33] M. Asefi and J. LoVetri, Use of field-perturbing elements to increase nonredundant data for microwave imaging systems, IEEE Trans. Microwave Theory Tech. **65**, 3172 (2017).

[34] A. C. T. Yoya, B. Fuchs, C. Leconte, and M. Davy, A reconfigurable chaotic cavity with fluorescent lamps for microwave computational imaging, Prog. Electromagn. Res. **165**, 1 (2019).

[35] P. del Hougne, M. Davy, and U. Kuhl, Optimal multiplexing of spatially encoded information across custom-tailored configurations of a metasurface-tunable chaotic cavity, Phys. Rev. Appl. **13**, 041004 (2020).

[36] P. del Hougne, M. Fink, and G. Lerosey, Shaping Microwave Fields Using Nonlinear Unsolicited Feedback: Application to Enhance Energy Harvesting, Phys. Rev. Appl. **8**, 061001 (2017).

[37] P. del Hougne, M. Fink, and G. Lerosey, Optimally diverse communication channels in disordered environments with tuned randomness, Nat. Electron. **2**, 36 (2019).

[38] P. del Hougne, M. F. Imani, T. Sleasman, J. N. Gollub, M. Fink, G. Lerosey, and D. R Smith, Dynamic metasurface aperture as smart around-the-corner motion detector, Sci. Rep. **8**, 6536 (2018).

[39] P. del Hougne, M. F. Imani, M. Fink, D. R. Smith, and G. Lerosey, Precise Localization of Multiple Noncooperative Objects in a Disordered Cavity by Wave Front Shaping, Phys. Rev. Lett. **121**, 063901 (2018).

[40] M. Davy, J. de Rosny, and P. Besnier, Green's Function Retrieval with Absorbing Probes in Reverberating Cavities, Phys. Rev. Lett. **116**, 213902 (2016).

[41] P. del Hougne and G. Lerosey, Leveraging Chaos for Wave-Based Analog Computation: Demonstration with Indoor Wireless Communication Signals, Phys. Rev. X **8**, 041037 (2018).

[42] The field ergodicity means that fields in chaotic systems are statistically equivalent to an appropriate random superposition of plane waves leading to a field which is statistically uniform,depolarized, and isotropic, i.e., the fields are specklelike [20,46,55,56,91,92].

[43] U. Kuhl, O. Legrand, F. Mortessagne, K. Oubaha, and M. Richter, Statistics of Reflection and Transmission in the Strong Overlap Regime of Fully Chaotic Reverberation Chambers, arXiv:1706.04873.

[44] R. Serra, A. C. Marvin, F. Moglie, V. M. Primiani, A. Cozza, L. R. Arnaut, Y. Huang, M. O. Hatfield, M. Klingler, and F. Leferink, Reverberation chambers a la carte: An overview of the different mode-stirring techniques, IEEE Electromagn. Compat. Mag. **6**, 63 (2017).

[45] D. A. Hill, *Electromagnetic Fields in Cavities: Deterministic and Statistical Theories*, IEEE Press Series on Electromagnetic Wave Theory (IEEE/Wiley, Piscataway/Hoboken, NJ, 2009).

[46] J.-B. Gros, U. Kuhl, O. Legrand, F. Mortessagne, and E. Richalot, Universal intensity statistics in a chaotic reverberation chamber to refine the criterion of statistical field uniformity, in *2015 IEEE Metrology for Aerospace (MetroAeroSpace), Benevento, 2015* (IEEE, Piscataway, NJ, 2015), pp. 225–229.

[47] A. Cozza, The role of losses in the definition of the overmoded condition for reverberation chambers and their statistics, IEEE Trans. Electromagn. Compat. **53**, 296 (2011).

[48] M. R. Schroeder and K. H. Kuttruff, On frequency response curves in rooms. Comparison of experimental, theoretical, and Monte Carlo results for the average frequency spacing between maxima, J. Acoust. Soc. Am. **34**, 76 (1962).

[49] The ERMs are placed on three contiguous and nonparallel cavity walls to avoid potentially nongeneric modes [22].

[50] N. Kaina, M. Dupré, M. Fink, and G. Lerosey, Hybridized resonances to design tunable binary phase metasurface unit cells, Opt. Express **22**, 18881 (2014).

[51] D. F. Sievenpiper, J. H. Schaffner, H. J. Song, R. Y. Loo, and G. Tangonan, Two-dimensional beam steering using an electrically tunable impedance surface, IEEE Trans. Antennas Propag. **51**, 2713 (2003).

[52] A. Sihvola, Metamaterials in electromagnetics, Metamaterials **1**, 2 (2007).

[53] A. Li, S. Singh, and D. Sievenpiper, Metasurfaces and their applications, Nanophotonics **7**, 989 (2018).

[54] J.-B. Gros, U. Kuhl, O. Legrand, F. Mortessagne, and E. Richalot, Review on chaotic reverberation chambers : theory and experiment (unpublished).

[55] Y.-H. Kim, Ulrich Kuhl, H.-J. Stöckmann, and P. W. Brouwer, Measurement of Long-Range Wave-Function Correlations in an Open Microwave Billiard, Phys. Rev. Lett. **94**, 036804 (2005).

[56] R. Pnini and B. Shapiro, Intensity fluctuations in closed and open systems, Phys. Rev. E **54**, R1032(R) (1996).

[57] C. Lemoine, P. Besnier, and M. Drissi, Investigation of reverberation chamber measurements through high-power goodness-of-fit tests, IEEE Trans. Electromagn. Compat. **49**, 745 (2007).

[58] B. Dietz, H.L. Harney, A. Richter, F. Schäfer, and H.A. Weidenmüller, Cross-section fluctuations in chaotic scattering, Phys. Lett. B **685**, 263 (2010).

[59] In Weyl's law applied to a 3D EM cavity, there is no term proportional to f and the total surface S of the cavity; hence, changing the configuration of an ERM is not expected to affect the cavity's mean density of states.

[60] B. Köber, U. Kuhl, H.-J. Stöckmann, T. Gorin, D. V. Savin, and T. H. Seligman, Microwave fidelity studies by varying antenna coupling, Phys. Rev. E **82**, 036207 (2010).

[61] Y. V. Fyodorov, D. V. Savin, and H.-J. Sommers, Scattering, reflection and impedance of waves in chaotic and disordered systems with absorption, J. Phys. A **38**, 10731 (2005).

[62] H. U. Baranger and P. A. Mello, Short paths and information theory in quantum chaotic scattering: transport through quantum dots, Europhys. Lett. **33**, 465 (1996).

[63] J. A. Hart, T. M. Antonsen, and E. Ott, Effect of short ray trajectories on the scattering statistics of wave chaotic systems, Phys. Rev. E **80**, 041109 (2009).

[64] J.-H. Yeh, J. A. Hart, E. Bradshaw, T. M. Antonsen, E. Ott, and S. M. Anlage, Experimental examination of the effect of short ray trajectories in two-port wave-chaotic scattering systems, Phys. Rev. E **82**, 041114 (2010).

[65] J.-H. Yeh, J. A. Hart, E. Bradshaw, T. M. Antonsen, E. Ott, and S. M. Anlage, Universal and nonuniversal properties of wave-chaotic scattering systems, Phys. Rev. E **81**, 025201(R) (2010).

[66] P. del Hougne, B. Rajaei, L. Daudet, and G. Lerosey, Intensity-only measurement of partially uncontrollable transmission matrix: demonstration with wave-field shaping in a microwave cavity, Opt. Express **24**, 18631 (2016).

[67] See Supplemental Material at http://link.aps.org/supplemental/10.1103/PhysRevA.101.061801 for a summary of key parameters of the considered modal overlap regimes and illustrations of universal vs nonuniversal behavior in our system.

[68] D. V. Savin, M. Richter, U. Kuhl, O. Legrand, and F. Mortessagne, Fluctuations in an established transmission in the presence of a complex environment, Phys. Rev. E **96**, 032221 (2017).

[69] Y. V. Fyodorov and D. V. Savin, Statistics of Resonance Width Shifts as a Signature of Eigenfunction Nonorthogonality, Phys. Rev. Lett. **108**, 184101 (2012).

[70] J.-B. Gros, U. Kuhl, O. Legrand, F. Mortessagne, E. Richalot, and D. V. Savin, Experimental Width Shift Distribution: A Test of Nonorthogonality for Local and Global Perturbations, Phys. Rev. Lett. **113**, 224101 (2014).

[71] C. Poli, G. A. Luna-Acosta, and H.-J. Stöckmann, Nearest Level Spacing Statistics in Open Chaotic Systems: Generalization of the Wigner Surmise, Phys. Rev. Lett. **108**, 174101 (2012).

[72] S. Kumar, A. Nock, H.-J. Sommers, T. Guhr, B Dietz, M. Miski-Oglu, A. Richter, and F. Schäfer, Distribution of Scattering Matrix Elements in Quantum Chaotic Scattering, Phys. Rev. Lett. **111**, 030403 (2013).

[73] The difference between both distributions is also visible on the bulk of the probability distribution function (see the insets of Fig. 3).

[74] C. Lemoine, P. Besnier, and M. Drissi, Advanced method for estimating number of independent samples available with stirrer in reverberation chamber, Electron. Lett. **43**, 861 (2007).

[75] M. Klingler, Dispositif et procédé de brassage électromagnétique dans une chambre réverbérante à brassage de modes, Patent No. FR 2,887,337 (2005).

[76] L. F. Wanderlinder, D. Lemaire, I. Coccato, and D. Seetharamdoo, Practical implementation of metamaterials in a reverberation chamber to reduce the luf, in *2017 IEEE 5th International Symposium on Electromagnetic Compatibility (EMC-Beijing), Beijing, 2017* (IEEE, Piscataway, NJ, 2017), pp. 1–3.

[77] J.-B. Gros, G. Lerosey, F. Mortessagne, U. Kuhl, and O. Legrand, Uncorrelated Configurations and Field Uniformity in Reverberation Chambers Stirred by Tunable Metasurfaces, arXiv:1905.12757.

[78] K. Rosengren and P.-S. Kildal, Radiation efficiency, correlation, diversity gain and capacity of a six-monopole antenna array for a MIMO system: theory, simulation and measurement in reverberation chamber, in *IEE Proceedings-Microwaves, Antennas and Propagation, 2005* (IET, London, 2005), Vol. 152, pp. 7–16.

[79] G. Gradoni, T. M. Antonsen, S. M. Anlage, and E. Ott, Random Coupling Model for interconnected wireless environments, in *2014 IEEE International Symposium on Electromagnetic Compatibility, Raleigh, NC, 2014* (IEEE, Piscataway, NJ, 2014), pp. 792–797.

[80] C. Lemoine, E. Amador, and P. Besnier, Mode-stirring efficiency of reverberation chambers based on rician k-factor, Electron. Lett. **47**, 1114 (2011).

[81] C. L. Holloway, H. A. Shah, R. J. Pirkl, W. F. Young, D. A. Hill, and J. Ladbury, Reverberation chamber techniques for determining the radiation and total efficiency of antennas, IEEE Trans. Antennas Propag. **60**, 1758 (2012).

[82] P. Hallbjörner, Reflective antenna efficiency measurements in reverberation chambers, Microw. Opt. Technol. Lett. **30**, 332 (2001).

[83] P. Besnier, C. Lemoine, J. Sol, and J.-M. Floc'h, Radiation pattern measurements in reverberation chamber based on estimation of coherent and diffuse electromagnetic fields, in *2014 IEEE Conference on Antenna Measurements & Applications (CAMA), Antibes Juan-les-Pins, 2014*, (IEEE, Piscataway, NJ, 2014), Vol. 6164, pp. 1–4.

[84] X. Chen, J. Tang, T. Li, S. Zhu, Y. Ren, Z. Zhang, and A. Zhang, Reverberation chambers for over-the-air tests: An overview of two decades of research, IEEE Access **6**, 49129 (2018).

[85] H. G. Krauthauser and M. Herbrig, Yet another antenna efficiency measurement method in reverberation chambers, in *2010 IEEE International Symposium on Electromagnetic Compatibility, Fort Lauderdale, FL, 2010* (IEEE, Piscataway, NJ, 2010), Vol. 3, pp. 536–540.

[86] E. Amador, H. G. Krauthauser, and P. Besnier, A binomial model for radiated immunity measurements, IEEE Trans. Electromagn. Compat. **55**, 683 (2013).

[87] H. G. Krauthauser, T. Winzerling, J. Nitsch, N. Eulig, and A. Enders, Statistical interpretation of autocorrelation coefficients for fields in mode-stirred chambers, in *2005 International Symposium on Electromagnetic Compatibility, Chicago, 2005. EMC 2005.* (IEEE, Piscataway, NJ, 2005), Vol. 2, pp. 550–555.

[88] C.L. Holloway, D.A. Hill, John Ladbury, G. Koepke, and R. Garzia, Shielding effectiveness measurements of materials using nested reverberation chambers, IEEE Trans. Electromagn. Compat. **45**, 350 (2003).

[89] P. Corona, A. de Bonitatibus, and E. Paolini, In Order to Evaluate in Reverberating Chamber the Radiated Power of Transmitting Equipments, in *1981 IEEE International Symposium on Electromagnetic Compatibility, Boulder, CO, 1981* (IEEE, Piscataway, NJ, 1981), pp. 1–2.

[90] Y. V. Fyodorov, S. Suwunnarat, and T. Kottos, Distribution of zeros of the *s*-matrix of chaotic cavities with localized losses and coherent perfect absorption: non-perturbative results, J. Phys. A: Math. Theor. **50**, 30LT01 (2017).

[91] U. Dörr, H.-J. Stöckmann, M. Barth, and U. Kuhl, Scarred and Chaotic Field Distributions in a Three-Dimensional Sinai-Microwave Resonator, Phys. Rev. Lett. **80**, 1030 (1998).

[92] S. Hemmady, X. Zheng, T. M. Antonsen, Jr., E. Ott, and S. M. Anlage, Universal statistics of the scattering coefficient of chaotic microwave cavities, Phys. Rev. E **71**, 056215 (2005).